JOURNAL OF SOLID STATE CHEMISTRY 88, 334–350 (1990)

Structural Analysis of Metastable Pseudobrookite Ferrous Titanium Oxides with Neutron Diffraction and Mossbauer Spectroscopy

RAYMOND G. TELLER AND MARK R. ANTONIO

BP Research, Warrensville Laboratory, 4440 Warrensville Center Road, Cleveland, Ohio 44128

ALPHONSO E. GRAU AND MICHEL GUEGUIN

QIT-Fer et Titane Inc., P.O. Box 560, Sorel, Quebec, Canada J3P 5P6

AND EDWARD KOSTINER

Department of Chemistry, University of Connecticut, Storrs, Connecticut 06269

Received February 12, 1990; in revised form May 11, 1990

Four synthetic iron titanium oxides with the pseudobrookite (AB_2O_5, *Cmcm*, $Z = 4$) structure have been prepared and characterized by neutron diffraction and zero-field, natural abundance ^{57}Fe Mossbauer effect spectroscopy (MES). The combination of the element specificity of MES with the different neutron scattering lengths of Ti and Fe (-0.33 and 0.95×10^{-12} cm, respectively) offers a unique opportunity to distinguish between cation distributions on the two ("*A*" and "*B*") sites. Two of the samples have been prepared in low temperature experiments (quenched from 1200°C) and have the stoichiometry $FeTi_2O_5$, and $Fe_{.6}Mg_{.6}Ti_{1.8}O_5$. The third and fourth samples are commercial iron titanium oxides prepared by the reduction of ilmenite ore with carbon above 1700°C. The stoichiometries of these samples are $Mn_{0.05}Fe_{0.33}Ti_{2.52}O_5$ and $Fe_{.33}Mg_{.31}Ti_{2.36}O_5$. Results from these experiments indicate that for each of these samples the *B* site is predominantly (>65%) occupied by Ti, while the *A* site contains a mixture of Ti, Fe, and/or Mg. However, only at higher temperatures (>1700°C) is the *B* site devoid of ferrous cations. These results suggest that an "ordered" model for ferrous titanium-rich oxides of the pseudobrookite structure (100% Ti occupancy of the *B* site) is descriptive only at elevated temperatures, and that at lower temperatures a "disordered" model (partial iron occupation of the *B* site) is a more accurate representation of the structure. Because of this difference, it may be possible to predict the thermal history of naturally occurring samples based on cation distributions.

Introduction

The iron titanium oxide phase diagram is rich in compounds ($FeTi_2O_5$, Fe_2TiO_5, Fe_2TiO_4, $FeTiO_3$, . . .), owing to the diversity of oxidation states of the cations (Fe^{2+}, Fe^{3+}, Ti^{4+}, Ti^{3+}) (1–7). Under reducing conditions it has been possible to quench synthetic metastable materials that contain Fe^{2+} and Ti^{3+} cations within the same oxide lattice (thermodynamically unstable at room temperature with respect to Fe^0, Ti^{4+}). The parent structure for these compounds is pseudobrookite, originally described by

0022-4596/90 $3.00

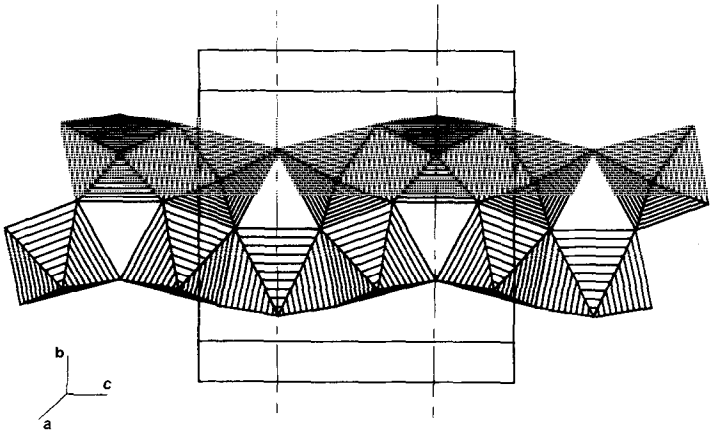

FIG. 1. Representation of the octahedral coordination polyhedra of the pseudobrookite (AB_2O_5) structure as viewed down a. A single chain of edge and corner-shared octahehra are shown. All cations lie on a mirror plane in the bc plane (at $a = 1/4$). A sites are located on lines defined by the intersection of this mirror plane with mirror planes in the ab plane (at $c = 1/4, 3/4$ indicated in the figure). A sites share octahedron edges with B sites in sets of three. B sites are on the outside of each set of three edge-shared octahedra. The structure is generated by translating these chains by 1/2 unit cell in the a and b directions. Outlines of the unit cell are shown.

Pauling (*2*). It was identified in the TiO_2–FeO phase diagram some time ago (*3*) and has since been identified as the structure for a number of titanium-containing compounds with the M_3O_5 stoichiometry (*4–7*). These materials have also been found in nature (*8, 9*) wherein a combination of reducing and rapid quenching conditions exist. Figure 1 contains a graphical representation of the pseudobrookite AB_2O_5 structure with 4 A and 8 B sites within the unit cell (one-half of the unit cell contents are shown).

This work describes the variety of metal cation distributions that can be accommodated by iron titanium oxide phases with the pseudobrookite structure synthesized under two different reducing conditions and temperatures. The decomposition of these metastable materials at elevated temperatures is also described. Accordingly, a total of four samples were prepared and characterized. Two materials (nominally $FeTi_2O_5$ and $(Fe_{.5}Mg_{.5})Ti_2O_5$) were prepared in a "low temperature" ($T = 1200$°C) synthesis, wherein the reducing conditions were strictly controlled; and two additional materials were prepared at higher temperatures ($T > 1700$°C) utilizing a commercial process wherein conditions as reducing as possible were maintained.

The four samples were characterized by powder neutron diffraction, and zero-field, natural abundance ^{57}Fe Mossbauer effect spectroscopy (MES) measurements; results are described here. In an accompanying article, a description of the chemistry and kinetics of the decomposition of the materials is given.

Neutron diffraction was utilized for this study because of the advantages this technique offers over X-ray diffraction: the most important of which is due to the difference in scattering physics between the two techniques. X-rays are scattered by electron density, and, since Ti and Fe are surrounded by approximately the same number of electrons, they are difficult to accurately distinguish in an X-ray diffraction experiment. In

neutron scattering experiments, however, nuclei scatter neutrons and the neutron scattering lengths of the elements in question (0.95×10^{-12} cm for Fe and -0.33×10^{-12} cm for Ti) differ significantly in magnitude and also have different signs. This makes characterizing the elemental distributions of the cation sites straightforward. Neutron diffraction analysis, combined with the element specificity of MES, is uniquely suited to decipher the cation distributions within the materials studied here. Conversely, the similarity of the X-ray scattering factor functions of Ti and Fe ensure that similar studies based on X-ray diffraction analysis will have considerably larger errors than results of neutron diffraction analysis discussed here.

Rietveld analysis (*10*), used to extract structural information from the neutron diffraction data, is a least-squares technique wherein crystallographic models for the structures present in the sample, in addition to models for the diffractogram background, Bragg peak shapes, scale factors, extinction, and absorption, are adjusted to fit the entire observed diffraction pattern. It is the strength of this technique to provide accurate structural data (assuming sufficient instrument resolution) on powdered samples. This information can also be obtained in the presence of additional phases.

Experimental

Synthesis of I and II were performed in sealed, evacuated quartz tubes. The presence of Fe in each tube controled the oxidation states of the metals in the product compounds.

Synthesis of (I) "$FeTi_2O_5$." Into a quartz tube was placed a mixture of 2.662 g of Fe_2O_3 (0.0167 moles), 0.931 g of Fe (0.0167 moles), and 7.990 g of TiO_2 (0.10 moles). This quartz tube was sealed under vacuum (100 mTorr) and placed in a furnace at 1200°C. After 16 hr (overnight), the tube was dropped from the furnace into an ice-water bath. X-ray diffraction analysis indicated the presence of ilmenite, pseudobrookite, and rutile phases. This mixture was then reground and once again placed in a sealed evacuated tube held at 1200°C, followed by an ice-water quench. This procedure was repeated until diffraction analysis indicated that there was no change in the phase composition of the resultant mixture. Phases corresponding to pseudobrookite and rutile (TiO_2 at approximately the 1 wt% level) structures are present in the final mixture. The total time at 1200°C was 48 hr.

Synthesis of (II) "$Fe_{.5}Mg_{.5}Ti_2O_5$." Into a quartz tube was placed 2.129 g of Fe_2O_3 (0.0133 moles), 0.745 g of Fe (0.0133 moles), 1.612 g of MgO (0.04 moles), and 12.784 g of TiO_2 (0.16 moles). The synthesis procedure was identical to that utilized for $FeTi_2O_5$ and was repeated until consecutive heat treatments showed no change (according to X-ray diffraction analysis). The total time at 1200°C was 58 hr. Phases corresponding to pseudobrookite and rutile (at approximately the 10–15 wt% level) were present at the conclusion of the procedure.

Samples slag III and slag IV are commercial iron (magnesium) titanium oxide compounds. The commercial preparation of these samples involves the reduction of ilmenite with carbon at elevated ($T > 1700$°C) temperatures. The process is roughly described by the following equation:

$$2FeTiO_3 + C \rightarrow CO + FeTi_2O_5 + Fe. \quad (1)$$

At the synthesis temperatures, molten Fe is easily separated from the slag ($FeTi_2O_5$). For samples III and IV, carbon in excess of that described by Eq. (1) was used in the reaction, producing a titanium-rich, $Fe_{1-x}Ti_{2+x}O_5$, material that is nearly 100% pure. X-ray diffraction analysis indicates that the major impurities in these samples are rutile and metallic iron (at very low levels, <1 wt%).

The difference between samples slag III

and slag IV is the presence of significant amounts of Mg in the starting material for IV and small amounts of Mn in III. Elemental analyses (XRF) of III and IV yield the following stoichiometries (based on 5 oxygen atoms): $Ti_{2.52}Fe_{0.33}Mn_{0.05}O_5$ and $Ti_{2.36}Fe_{0.33}Mg_{0.31}O_5$, respectively.

Neutron diffraction measurements. Time-of-flight (TOF) neutron diffraction data were collected at ambient temperature and pressure at Argonne National Laboratory with the IPNS (Intense Pulsed Neutron Source) on the special environment powder diffractometer (SEPD) or the general purpose powder diffractometer (GPPD). Data from the backscattering detectors ($2\Theta = 150°$) were used in the refinements as this is the highest resolution data available from each instrument (ca. 0.3%). In the TOF technique, the sample, detector, and source are fixed and neutrons of differing wavelengths are detected. The data are binned from 5000 to 30,000 in 5-μsec intervals ($\Delta d = 5 \times 10^{-5}$ for the GPPD, $\Delta d = 7 \times 10^{-5}$ for the SEPD). Each sample was contained within a 1/2-in.-diameter seamless vanadium tube, capped at both ends with aluminum plugs. Details of the instrument and the data collection and data analysis software package have been previously published (*11*). Analysis of the data was performed with a Rietveld profile least-squares program adapted for time-of-flight neutron data and multiphase samples. Starting structural parameters for the least-squares process were taken from the open literature. For the ferrous pseudobrookite structure, a crystallographic model isostructural with that of ferric pseudobrookite was chosen (*2*) (*Cmcm*, two metal sites, metal atoms at 4*c* 100% Ti, 0% Fe = 0.0, 0.19, 0.25, and 8*f* 50% Ti, 50% Fe = 0.0, 0.135, 0.56.) In the following discussion, the 4*c* cation site is designated as "*A*" and the 8*f* cation site as "*B*." The same model was chosen for the magnesium-ferrous pseudobrookite phase. In the least-squares refinement, only the scale factors and background parameters were initially allowed to vary. Upon convergence, more parameters were allowed to vary until, for the final cycles of refinement, all reasonable parameters were allowed to vary. They include thermal and atomic positional parameters, unit cell constants, background, absorption, extinction, and peak shape parameters. In addition to these, occupation parameters of the metal sites were also allowed to vary as if each were a Ti atom. This is equivalent to refining the scattering length because the algebraic sum of the individual scatterers can be readily calculated. The oxygen sites were assumed to be 100% occupied. Scattering lengths used in subsequent calculations are -0.33 for Ti, 0.95 for Fe, 0.52 for Mg, -0.36 for Mn, and 0.575 ($\times 10^{-12}$ cm) for O.

After analysis of the diffraction data, the Mossbauer effect data (vide infra) were analyzed. Based on these data, a model for three cations distributed over the two distinct crystallographic oxygen octahedra was considered. Initially, both the thermal parameters for the cation sites in $FeTi_2O_5$ and $FeMgTi_4O_{10}$ were allowed to vary aniostropically. The shape of these resulting thermal ellipsoids suggested that for the *A* sites there could be two distinct cation sites within the oxygen octahedron. Accordingly a model was refined that placed two (half weighted) isotropically vibrating nucleii within the *A* octahedron separated by 0.5 Å in positions. Least-squares refinement of these models for data sets I and II converged to models in which there were two distinct cation sites within the "*A*" octahedron of oxygen atoms. However, the estimated standard deviations in the atomic positional parameters of these sites indicated that they were not significantly different. Therefore a model consisting of only two crystallographic cation sites is applicable.

For samples I and II small amounts of rutile (TiO_2) and for slag IV metallic iron were detected. Cell, positional (rutile), and

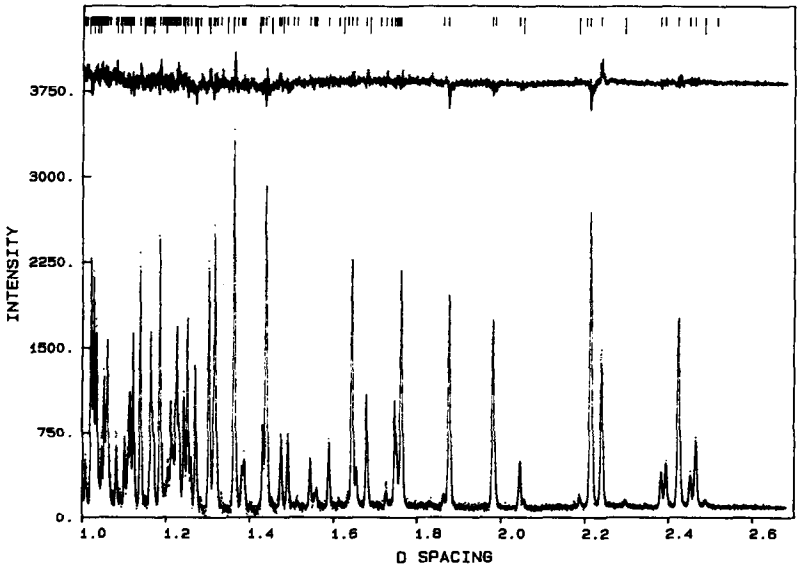

FIG. 2. A portion of the neutron diffraction data for sample I. Raw data are represented by points, and the calculated plot by a line. A difference plot is presented at the top of the figure. Tick marks indicate the positions of Bragg peaks. Note that two phases are evident. Bragg peaks from the majority phase (pseudobrookite) are indicated by short tick marks, whereas those from rutile by long tick marks.

thermal parameters for this phases were also allowed to vary. All refinements converged rapidly. Final plots showing the raw diffraction data, calculated data, and difference plots are given in Figs. 2–5.

Mossbauer effect measurements. The zero-field, natural abundance iron-57 Mossbauer effect data were collected on the finely powdered samples (I–IV), supported between boron nitride plates (1 in.-diameter × 0.025 in.-thick PDS BN-975, Standard Oil Engineered Materials). The sample masses (ca. 0.26–0.39g) were adjusted to obtain thin absorbers, ca. $1.04–1.17/(\mu/\rho)$, where μ/ρ is the nonresonant electronic mass absorption coefficient (cm^2/g) at 14.41 keV (*12*). A Ranger Scientific MS-900 Mossbauer effect spectrometer was employed for transmission measurements. The source (ca. 10 mCi cobalt-57 diffused into rhodium foil; Amersham) and samples were maintained at room temperature. The MS-900 was operated in the constant-acceleration mode using a triangular (symmetric) waveform to drive the Ranger Scientific VT-1200 velocity transducer. Velocity calibration over the range 0 ± 6 mm/sec was maintained by use of a natural iron, α-Fe, absorber foil (0.025 mm thick); all isomer shifts are quoted relative to natural iron at room temperature. The zero velocity calibration (i.e., 0 mm/sec isomer shift) was taken as the midpoint of the inner four reasonances of the iron foil. A linear velocity scale was used for the velocity per channel (mm/sec/ch) conversion over the entire range. A Reuter–Stokes proportional counter (fill gas: 97% Kr–3% CO_2), fitted to a Ranger Scientific preamplifier (PA-900) and 1024 channel multichannel analyzer/scaler, was used for the γ-ray detection. The entire MS-900 system was controlled with an IBM AT personal computer. All Mossbauer effect data were recorded to a suitable background level of ca. 700,000 counts per channel (before folding). The primary experimental data were first folded

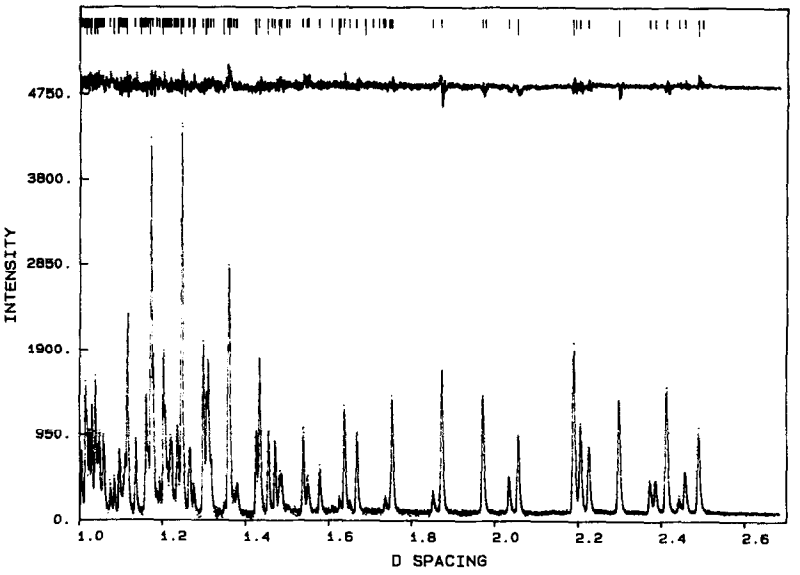

FIG. 3. Neutron data for sample II. Raw data are represented by points, and the calculated plot by a line. A difference plot is presented at the top of the figure. Tick marks indicate the positions of Bragg peaks. Note that two phases are evident. Bragg peaks from the majority phase (pseudobrookite) are indicated by short tick marks, whereas those from rutile by long tick marks.

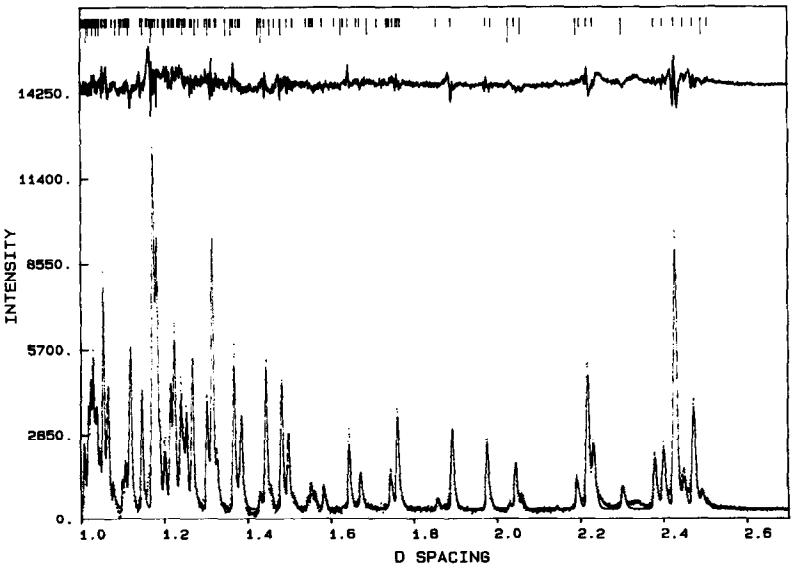

FIG. 4. Neutron data for slag III. Data are presented as in the legends to Figs. 2 and 3. Bragg peak positions for iron (a trace impurity) are indicated with the longest tick marks.

and then fit with both Lorentzian line shapes and additive Lorentzian and Gaussian line shapes. Estimated standard deviations for isomer shifts, quadrupole splittings, and FWHM (full width at half maximum) line widths are 0.02 mm/sec.

Results and Discussions

The phases present in materials isolated from the commercial production of titania slags have been described elsewhere (*13*). In addition to a titanium-rich pseudobrookite phase, $M_{1-x}Ti_{2+x}O_5$ (M = Fe, Mg), very small amounts of iron, iron sulfide, ulvospinel (Fe_2TiO_4), and an amorphous silicate phase are also present in slags III and IV. Despite the differences in synthesis conditions, all four of the samples discussed herein are similar in that the major phase of each is of the pseudobrookite structure. Table II summarizes the diffraction data on samples I–IV. In contrast to the slag samples, the only impurities in I and II are TiO_2 (estimated to be approximately 1 and 10–15 mol%, respectively), and traces of metallic iron (detected by MES). The materials prepared here are metastable phases at room temperature and their synthesis requires quenching from elevated (>1200°C) temperatures. This is confirmed by the conditions required for the synthesis of these materials. For example, mixtures of Fe, Fe_2O_3, and TiO_2 (molar ratio 1 : 1 : 6) that are allowed to cool to room temperature from 1200°C over a period of hours yield a mixture of $FeTiO_3$ and TiO_2: no pseudobrookite phase is detected by X-ray diffraction. Quenching the same mixture from 1200°C produces a material with pseudobrookite as its major constituent (by X-ray diffraction). These observations are consistent with thermodynamic estimates of the stability of $M^{2+}Ti_2O_5$ materials. For example, it has been shown that at temperatures below 1400°K, $FeTi_2O_5$ is unstable with respect to $FeTiO_3$ and TiO_2 (*14*). Accordingly, for the four samples analyzed in this report conditions were chosen to provide the most rapid quenching possible.

The gross structural features of the pseudobrookite (AB_2O_5) structure have been reported (*4–7*). While the nearest cations (second nearest neighbors) to the B sites are both A and B cations, the eight nearest (within 3.25 Å) cations to the A sites are all B sites. Figure 1 shows a representation of the structure, which is related to the rutile structure. Removing oxygens from the rutile structure (stoichiometry MO_2) and introducing shear planes gives rise to the pseudobrookite structure (*15*) (stoichiometry M_3O_5). The metal oxygen octahedra of this structure are quite asymmetric (see Table IV for a listing of bond distances in the materials studied here), and a number of cations of differing oxidation states can be accommodated in the structure. For example, Ti_3O_5, Fe_2TiO_5, $Fe_{1-x}Ti_{2+x}O_5$ ($.76 > x > 1$), and $(Mg_{1-x}Fe_x)Ti_2O_5$ ($0 < x < 1$) have the pseudobrookite structure. A number of synthetic and naturally occurring iron titanium and iron-magnesium titanium oxides having the pseudobrookite structure with differing cation distributions have been described in the literature (*1, 2, 4–8*). Some of this structural work is noteworthy and will be discussed in detail.

Wechsler (*6*) has used single crystal X-ray diffraction data to characterize single crystals of a material isolated from a mixture of composition Fe/Mg/Ti/O/ = 1/1/4/10 at elevated temperatures. In a least-squares analysis of the diffraction data, the occupancies of Fe and Mg were arbitrarily constrained to be identical (this fixes the Fe and Mg occupancies to be the same on each cation site). In a quenched sample, Wechsler reports the distribution of cations to be 33.2% Fe, 33.2% Mg, and 33.5% Ti on the A site and 8.4% Fe, 8.4% Mg, and 83.2% Ti on the B site (*6*). After heating the sample to 1100°C, Wechsler further reports that the B site becomes slightly more Ti rich (occu-

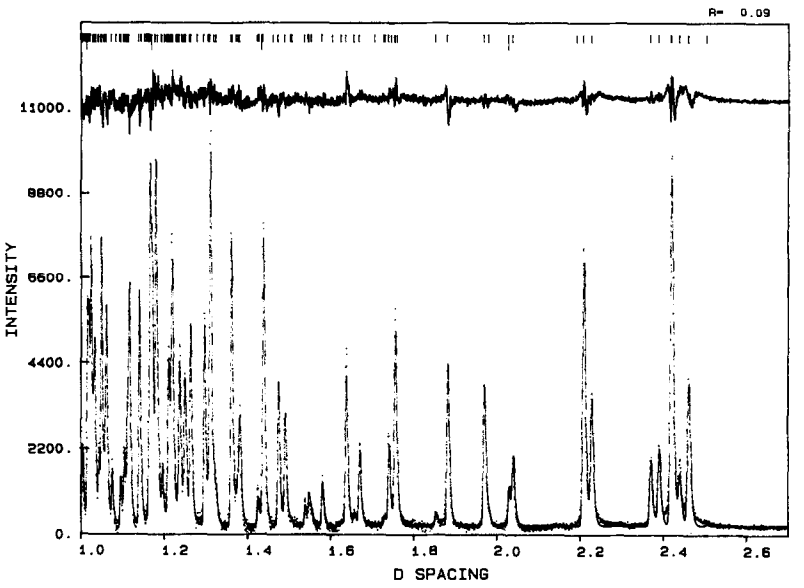

FIG. 5. Neutron data for slag IV. Data are presented as in the legends to Figs. 2 and 3. No rutile was detected in this sample. The major peaks for the only impurity phase detected with the diffraction data (iron) are indicated in the figure with long tick marks. This phase was not included in the fit.

TABLE I

RESULTS OF RIETVELD REFINEMENTS FOR I, II, AND SLAGS III AND IV[a]

	I	II	Slag III[b]	Slag IV[b]
$R_{w\ prof}$(%)	5.1	4.9	6.6	7.4
R_{prof}(%)	3.8	3.6	4.2	4.6
$R_{expect.}$(%)	3.5	3.6	2.1	2.8
Data/parameter ratio	169	142	145	122
Data d-range (Å)	0.6–2.7	0.6–2.7	0.8–3.6	0.9–3.6
sig_0[c]	−0.68	−1.34	−0.93	−0.80
sig_1	7.6	9.4	10.3	11.6
a_{Rutile}(Å)	4.594(2)	4.5938(3)	4.6015(3)	—
c_{Rutile}(Å)	2.959(2)	2.9595(3)	2.9647(3)	—
a_{Iron}(Å)	—	—	2.870(4)	—

[a] Pseudobrookite phase, space group $Cmcm$, $Z = 4$, rutile phase space group $P4_2/mnm$, $Z = 2$, iron phase space group $Im3m$, $Z = 2$. Unit cell constants are given in Table VI.

[b] A trace of iron metal was noted in this sample.

[c] Broadening of the function describing the Bragg peak profile (sig) is a function of d-value and is given by sig = sig0 + sig1 * d. The peak shape is a convolution of this function with two exponential (instrumentally determined) functions.

TABLE II

FINAL ATOMIC PARAMETERS FOR THE PSEUDOBROOKITE PHASES

	Pseudobrookite I ("$FeTi_2O_5$")			Pseudobrookite II ("$FeMgTi_4O_{10}$")		
Atom	x	y	z	x	y	z
A(4*c*)[a]	0	.1912(2)	1/4	0	.1909(4)	1/4
B(8*f*)	0	.1343(4)	.5627(4)	0	.127(9)	.527(5)
O_1	0	.7801(2)	1/4	0	.7685(2)	1/4
O_2	0	.0462(1)	.1145(1)	0	.0472(2)	.1157(1)
O_3	0	.3135(1)	.0636(1)	0	.3110(1)	.0690(1)
	Slag III			Slag IV		
A(4*c*)	0	.1775(23)	1/4	0	.1914(11)	1/4
B(8*f*)	0	.1353(3)	.5631(4)	0	.1346(4)	.5636(4)
O_1	0	.7772(2)	1/4	0	.7777(3)	1/4
O_2	0	.0457(2)	.1161(2)	0	.0440(2)	.1152(2)
O_3	0	.3133(2)	.0657(2)	0	.3139(2)	.0637(2)

Thermal parameters[b]

Atom site	B_{11}	B_{22}	B_{33}	B_{12}	B_{13}	B_{23}
I-*A*	.0073(9)	.0005(2)	.0007(1)	0	0	0
I-*B*	.0029(22)	.0018(4)	.0019(4)	0	0	.000(3)
II-*A*	.0061(19)	.0010(3)	.0011(3)	0	0	0
II-*B*	−.004(19)	.015(6)	−.005(3)	0	0	−.01(3)
III-*A*,*B*	0.55(8)					
IV-*A*,*B*	0.40(9)					

[a] The atomic positions for the rutile (TiO_2) phases are not extraordinary and are not reported here.

[b] Cations for I and II were modeled with anisotropic thermal parameters. For I and II the oxygen thermal parameters were constrained to be identical (converging to 0.95(4) and 0.83(3), respectively). For III and IV isotropic thermal parameters for all atoms were used, and the oxygen atom values converged to 0.40(3) and 0.51(3) for III and IV, respectively.

pancy = 91%) at the expense of the *A* site (*6*). Unfortunately, this is a compromised experiment. As noted above, X-ray diffraction data are not particularly sensitive to the distribution of Ti and Fe in oxides. The similarity of the scattering of X-rays by Fe and Ti makes it extremely difficult to distinguish these elements even in a well-designed X-ray scattering experiment without using radiation near the absorption edge of one of the two elements. Additionally, the data collected on the samples was of marginal quality (80% decomposition of the crystal was noted at the termination of the experiment) and apparently no analysis was made to determine the composition of the crystal (the cation composition in the least squares was constrained to adhere to 1 : 1 : 4, Fe/Mg/Ti). This latter fact is noteworthy because our work has shown that mixtures of the molar ratio Mg/Fe/Ti/O 1/1/4/10 when held at 1200°C yield TiO_2 and a titanium-poor $Mg_{.5+x}Fe_{.5+x}Ti_{2-2x}O_5$ phase.

Smyth (*5*) has used single crystal and microprobe analysis of crystals isolated from polished sections of moon rocks to attempt to determine the cation distributions in naturally occurring magnesium ferrous pseudo-

brookite phases. In the subsequent least-squares analysis of his single crystal data set, Smyth considered three models: (1) an "ordered" model (50% Fe, 50% Mg on the *A* site; 100% Ti on the *B* site); (2) a "disordered" model (17% Fe, 16% Mg, 67% Ti on the *A* site; 17% Fe, 16% Mg, 67% Ti on the *B* site), and (3) a "deficient" model (48% Mg on the *A* site; 100% Ti on the *B* site). Of these three models, Smyth determined that the ordered model gave the best fit to the diffraction data. In addition to suffering from a lack of sensitivity of Fe and Ti distributions inherent to X-ray diffraction data, this analysis only provides information about the three cation distributions considered. Rather than providing evidence for the "ordered" model, it can, at best, only eliminate the other two models considered.

In the results discussed below, it will be shown that the application of neutron diffraction and Mossbauer effect spectroscopy to ferrous titanium oxides of the pseudobrookite structure eliminates the uncertainties inherent in the X-ray diffraction work discussed above.

Mossbauer effect data. The zero-field, natural abundance ^{57}Fe Mossbauer effect spectra for samples I and II and slags III and IV are shown as the dotted curves in Figs. 6a, 6b, 6c, and 6d, respectively. Analyses of these spectra reveal three different ferrous ion sites for samples I and II, and two different ones for slags III and IV. Furthermore, for slags III and IV, the Mossbauer effect data reveal a trace amount of metallic iron, and, for sample II, a trace ferric impurity. These data were fit with three doublets (I and II) and two doublets (slags III and IV) of fully Lorentzian line shapes. The Lorentzian fits shown in Figs. 6a–6d as solid curves are clearly inadequate near the baseline on the low and high velocity edges of the intense resonances at ca. −0.5 and 2.6 mm/sec, respectively. Also, the minimum between the two intense, asymmetric resonances at ca. 0.0 and 2.0 mm/sec for sample I is not particularly fitted well. A significant improvement in the goodness of fits was obtained through statistical optimization of the line shape for each spectrum. An additive Lorentzian–Gaussian line shape, with an optimum Lorentzian contribution of some 60% and a Gaussian contribution of 40%, was found to produce excellent fits to the ferrous ion doublets. Similar line shape fitting effects were noted in an ^{57}Fe MES study of ferrous/ferric ion ratios in borosilicate glasses: the most ferrous-containing glasses had the greatest Gaussian contribution (ca. 40%) to the line shape of the quadrupole split Fe^{2+} doublets (*16*).

The pertinent Mossbauer effect parameters (i.e., isomer shifts, quadrupole splittings, and line widths) from the fully Lorentzian fits are presented in Table III along with those data of Grey and Ward (*1*). The corresponding parameters from the fits with Lorentzian–Gaussian line shapes were not significantly different from those in Table III. The data of Table III reveal both similarities and differences in the coordination of Fe^{2+} in the four samples. The common features of samples I and II are the occurrence of three similar quadrupole split doublets. Since no other iron-containing phases have been identified from the diffraction data (only pseudobrookite and rutile phases are observed), this suggests that there are three ferrous ion sites in the pseudobrookite phase. However, the commonly accepted structural model for pseudobrookite phases contains two cation sites and this has been confirmed with the diffraction data analysis described herein. A possible explanation of this apparent discrepancy lies in the interaction between the ferrous ions located on the *A* site and the *A* site second nearest neighbors. As discussed above, the eight nearest *A* site cations are all *B* cations, and two quadrupole split doublets would result from ferrous ions at the *A* site if there were two different average distributions of *B* cations (i.e., Ti and Fe for I; Mg, Ti, and Fe for II)

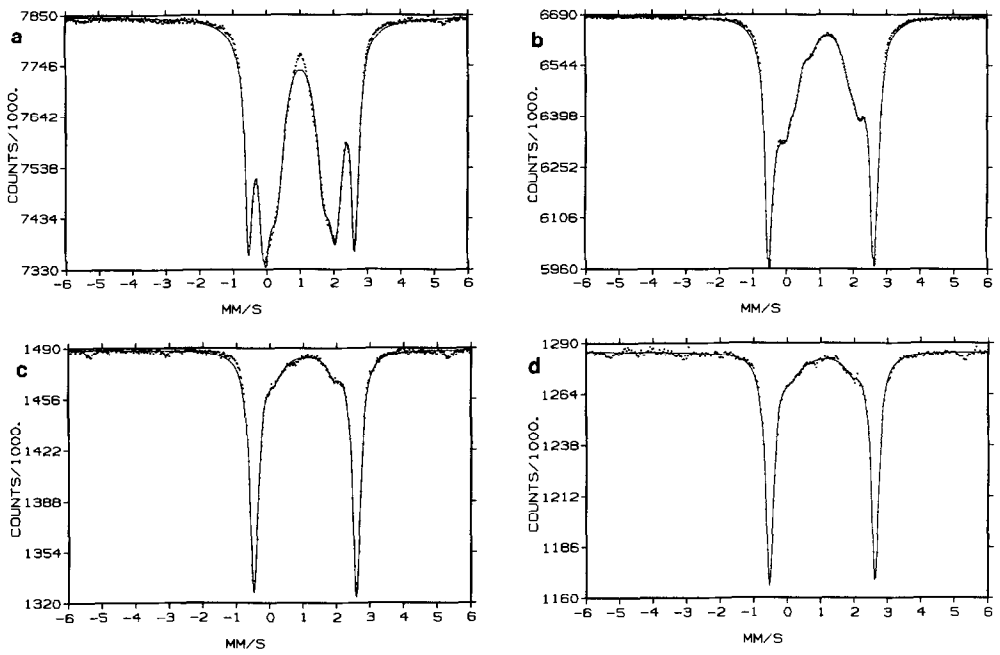

FIG. 6. ^{57}Fe Mossbauer effect data for (a) sample I, (b) sample II, (c) slag III, and (d) slag IV. Raw data is represented by points, and calculated data by a line. The calculated data was obtained from a least-squares fit of fully Lorentzian line shapes to the raw data. For a and b (I and II, respectively), the data is best fit by three quadrupole split doublets, and for c and d (slags III and IV, respectively) by two quadrupole split doublets with a 60% Lorentzian–40% Gaussian line shape.

about the *A* site. ^{57}Fe Mossbauer effect data recorded by Grey and Ward (*1*) for materials whose compositions are similar to those discussed here (see Table III) provide support for this model.

Based on this analysis and consideration of the neutron diffraction data (vide infra), we assign the three quadrupole split doublets of samples I and II to two ferrous sites within the pseudobrookite structure: one is the *B* site, and the other is the *A* site, which apparently has two different *B* cation distributions about it. This model implies that there may be some short-range order about the *A* site that is not reflected in the Bragg data.

As shown in Figs. 6c and 6d, the Mossbauer effect spectra for slags III and IV, respectively, share common features as well. Each spectrum consists of two quadrupole split doublets with similar isomer shifts and quadrupole splittings (see Table III). The intense, outer doublets are identical to those for I and II, and are characteristic of high-spin Fe^{2+}, d^6, ions in the pseudobrookite lattice. The weak, inner doublets are typical of ulvospinel, Fe_2TiO_4 (*17*). Under the high temperatures and reducing conditions employed in the ilmenite ore smelting process, it is easy to envision the production of minor amounts of this reduced material.

The common feature of all four ^{57}Fe Mossbauer effect spectra (cf. Figs. 6a–6d) is a quadrupole split doublet with an isomer shift of ca. 1.06 mm/sec and a quadrupole splitting of ca. 3.16 mm/sec. Since the common phase for all samples is pseudobrookite, this

TABLE III

RESULTS OF LEAST-SQUARES FITS OF LORENTZIAN LINE SHAPES TO MOSSBAUER EFFECT DATA[a]

Sample	Fourfold (*A*) site			Fourfold (*A*) site			Eightfold (*B*) site		
	Isomer shift[b]	Quad. split	FWHM	Isomer shift[b]	Quad. split	FWHM	Isomer shift[b]	Quad. split	FWHM
I	1.06	3.16	0.27	1.01	2.12	0.49	1.01	1.37	0.54
Rel. populations[c]		30			42			28	
II	1.06	3.14	0.30	1.07	2.20	0.49	1.05	1.63	0.45
Rel. populations[c]		58			28			14	
slag III[d]	1.06	3.07	0.30						
slag IV[d]	1.05	3.16	0.28						
	Isomer shift[b]	Quad. split	FWHM	Isomer shift[b]	Quad. split	FWHM	Isomer shift[b]	Quad. split	FWHM
$FeTi_2O_5$[e]	1.07[e]	3.24	0.29	1.04[e]	2.19	0.94			
$Fe_{0.2}Ti_{2.8}O_5$[e]	1.08[e]	2.85	0.35	1.01[e]	2.19	0.37	1.06[e]	1.36	0.35

[a] Units for isomer shift, quadrupole splitting, and FWHM line widths are millimeters per second. Estimated standard deviations for these parameters are 0.02 mm/sec.

[b] All isomer shifts are relative to natural iron, α-Fe, at room temperature.

[c] Based on integrated areas of the doublets. Estimated standard deviations are 5%.

[d] For slags III and IV, two other iron environments were observed in the Mossbauer effect spectra: (1) a doublet pattern (isomer shift = 1.03, quadrupole splitting = 1.80) characteristic of ulvospinel, Fe_2TiO_4, and a sextet pattern with an isomer shift (0.0 mm/sec) and magnetic hyperfine interaction that are characteristic of elemental iron. This latter assignment is in agreement with the diffraction data.

[e] Data from Ref. (*1*). The quadrupole splitting values reported in Ref. (*1*) have been doubled to correspond to the convention utilized here. To facilitate the comparison of isomer shifts reported in Ref. (*1*) (with a ^{57}Co/Pd source) with those reported here (^{57}Co/Rh source), 0.15 mm/sec was added to those data of Ref. (*1*). $FeTi_2O_5$ from Ref. (*1*) is of the pseudobrookite structure; $Fe_{0.2}Ti_{2.8}O_5$ is monoclinic with three crystallographically distinct metal sites.

confirms the assignment of this doublet to one cation site (*A* site) in the pseudobrookite lattice. The major difference between the Mossbauer effect data for the four samples (ignoring nonpseudobrookite phases) is the existence of three Fe^{2+} quadrupole split doublets for each of I and II and only one for slags III and IV. This result demonstrates that whereas the ferrous ions in III and IV are located on a single cation site within the pseudobrookite structure, they are distributed over both cation sites for I and II.

Neutron diffraction data. Table IV lists the neutron scattering lengths of the two observed pseudobrookite cation sites of samples I–IV. An examination of the calculated data at the bottom of Table IV clearly illustrates the advantage in using neutron diffraction data to distinguish site compositions in these materials. The total neutron scattering length of each site is determined by the algebraic sum of the individual scatterers occupying that site. Due to the wide disparity in scattering lengths of Fe and Ti atoms, the site scattering length accurately indicates the elemental composition. Models with differing cation occupations in the AB_2O_5 structure are illustrated at the bottom of Table IV. Examination of these model

TABLE IV

METAL DISTRIBUTIONS OF CATION SITES IN AB_2O_5 FROM NEUTRON DIFFRACTION DATA

Sample/AB_2O_5 stoichiometry[a]	A site ($\times 10^{12}$ cm) scattering length	B site ($\times 10^{12}$ cm) scattering length
A. Experimental data[a]		
I	0.57(1)	−0.18(1)
$(Fe_{.70}Ti_{.30})(Fe_{.23}Ti_{1.77})O_5$	(0.57)	(−0.18)
II	0.34(1)	−0.02(1)
$(Fe_{.5}Ti_{.5})(Mg_{.6}Fe_{.1}Ti_{1.3}))O_5$[b]	(0.31)	(−0.01)
Slag III	0.09(1)	−0.33(1)
$(Mn_{.05}Fe_{0.33}Ti_{0.52})(Ti_{2.00})O_5$	(0.12)	(−0.33)
Slag IV	0.26(1)	−0.29(2)
$(Mg_{.21}Fe_{.33}Ti_{.46})(Ti_{1.90}Mg_{0.1})O_5$	(0.28)	(−0.29)
B. Calculated data on model compounds		
$FeTi_2O_5$	0.95	−0.33
$MgTi_2O_5$	0.52	−0.33
$Ti(FeTi)O_5$	−0.33	0.62
$(Fe_{.9}Ti_{.1})(Fe_{.1}Ti_{1.9})O_5$	0.82	−0.27

[a] Experimentally determined scattering lengths (assuming 100% cation and anion occupancy) are given with estimated standard deviations in parentheses. Neutron scattering lengths are ($\times 10^{12}$ cm) Fe, 0.95; Mg, 0.52; Ti, −0.33; Mn, −0.36. Total unit cell scattering lengths for the model compounds are calculated by multiplying the site scattering length by 4 (A site) or 8 (B site). The scattering lengths given in parentheses under the experimentally determined values are those calculated based on the compositions given in the table.

[b] Reliance on the Mossbauer effect data to determine the relative ratios of iron located on the A and B sites reduces the precision of the cation distribution for this material.

compounds indicates that even small differences in cation distribution (such as $FeTi_2O_5$ versus $(Fe_{.9}Ti_{.1})(Ti_{1.9}Fe_{0.1})O_5$) can easily be distinguished.

Cation–oxygen distances are reported in Table V. The gross symmetries of the two cation sites are preserved in the four compounds examined here. The B site (m symmetry) and the A site (mm symmetry) are both significantly distorted from ideal octahedral symmetry. Sample II and slag IV are similar in cation sizes (Table V) and unit cell dimensions (Tables I and VI). This is not surprising in light of the similarities in composition of the compounds. It is interesting to note that the large difference in neutron scattering lengths between Fe and Ti, which allows the precise determination of cation distributions, can be detrimental in determining accurate cation–oxygen distances. This is especially true in those cases where the algebraic sum of the scattering lengths approaches zero, as is realized for the B site in sample II ("$FeMgTi_4O_{10}$," see Table IV). Since the total scattering length of this site is quite small (−0.02), the resultant cation–oxygen distances are determined imprecisely. Compared to the other three samples, it is noteworthy that the A site of the slag III sample is the largest, and the most distorted. This material also possesses the largest unit cell (see Table I).

Cation distributions within the pseudobrookite structure. The first conclusion to

TABLE V

CATION–OXYGEN DISTANCES (IN Å) IN SAMPLES I–IV (AB_2O_5)

	"$FeTi_2O_5$" I	"$FeMgTi_4O_{10}$" II	$Mn_{.05}Fe_{.33}Ti_{2.57}O_5$ Slag III	$Mg_{.31}Fe_{.32}Ti_{2.37}O_5$ Slag IV
A site[a]	1.968	1.942	1.862	1.972 (×2)
M–O	2.068	2.017	2.128	2.061 (×2)
	2.227	2.156	2.278	2.156 (×2)
Average	2.087	2.038	2.119	2.063
$d_{max} - d_{min}$	0.26	0.21	0.42	0.18
B site[b]	1.847	1.9	1.851	1.818
M–O	2.068	2.017	2.128	2.061 (×2)
	1.981	1.6	2.000	1.997
	2.064	2.4	2.061	2.054
	2.170	2.0	2.169	2.164
Average	1.991	2.0	1.999	1.998
$d_{max} - d_{min}$	0.32	0.8	0.32	0.35

[a] Estimated standard deviations for metal oxgen distances is 0.003–0.006 in all cases except for the *B* site of $FeMgTi_4O_{10}$. The *A* site possess *mm* symmetry, the *B* site *m* symmetry.

[b] Because the total scattering length of the *B* site for $FeMgTi_4O_{10}$ is significantly smaller than the scattering lengths of any of the other sites (see Table IV), the estimated standard deviation for the reported bond distance is much greater (by approximately 50).

be drawn regarding cation distributions based on the neutron diffraction data (Table IV) is that for all the samples of this study, the *B* site is predominantly occupied by Ti. Only for the slag samples (III and IV), however, is the scattering length of the *B* site sufficiently negative to justify assigning this site to be 100% or almost 100% Ti occupied. Therefore, only slags III and IV can be described as having an "ordered" (*5, 6*) cation distribution (*B* site 100% Ti), whereas the other two samples examined here are all, to some degree, "disordered" (*B* site significantly less than 100% Ti).

TABLE VI

COMPARISON OF THE LATTICE PARAMETERS OF I–IV TO LATTICE PARAMETERS OF $Fe_{1-x}Ti_{2+x}O_5$ FROM REF. (*1*)

Composition	*a*(Å)	*b*(Å)	*c*(Å)	*c*/*a*	Volume (Å^3)
I ("$FeTi_2O_5$")	3.7498	9.8057	10.0675	2.685	370.17
II ("$FeMgTi_4O_{10}$")	3.7413	9.7659	9.9946	2.671	365.17
Slag III	3.7828	9.7938	10.0280	2.651	371.52
Slag IV	3.7629	9.7556	10.0151	2.662	367.65
From Ref. (*1*)					
$FeTi_2O_5$	3.757	9.790	10.079	2.683	370.7
$Fe_{.9}Ti_{2.1}O_5$	3.763	9.794	10.054	2.672	370.5
$Fe_{.73}Ti_{2.27}O_5$	3.771	9.792	10.051	2.665	371.1
$Fe_{.66}Ti_{2.34}O_5$	3.782	9.788	10.041	2.656	371.6
$Fe_{.5}Ti_{2.5}O_5$	3.781	9.798	10.020	2.650	371.2
$Fe_{.45}Ti_{2.55}O_5$	3.785	9.798	10.013	2.645	371.3

By judicious use of the diffraction and Mossbauer effect data, cation distributions in these materails can be ascertained. For I ("$FeTi_2O_5$"), since only two cations (Fe, Ti) are present, calculation of the cation distributions on the basis of the neutron data is straightforward. The results reported in Table IV assume no cation or anion vacancies. Based on this distribution, the Mossbauer effect reasonances can be assigned. The doublet with the largest quadrupole splitting is assigned to the *A* site (this is the only Fe^{2+} site in the pseudobrookite lattice noted by use of MES for slags III and IV, and the diffraction data clearly place iron at this site). In order for the MES populations to agree with Fe/Ti distributions as determined by the neutron data, the Mossbauer effect resonances with the next largest quadrupole splitting must also be assigned to ferrous ions within the *A* octahedron of oxygen anions. The remaining doublet is assigned to a single site within the *B* octahedron.

For sample II, the distribution of three cations between two sites presents an apparently unsolvable algebraic problem for the neutron data. However, now that the Mossbauer effect signals have been assigned, the distribution of ferrous ions between the *A* and *B* sites can be assigned. By constraining the *A* site to have approximately six times the ferrous population as the *B* site (*18*), the diffraction data can be used to assign cation distributions. The approximate stoichiometry is presented in Table IV.

For slag III, the similarity of Mn and Ti neutron scattering lengths (-0.36×10^{-12} and -0.33×10^{-12} cm, respectively) makes the assignment of cation distributions on the basis of site scattering lengths alone impossible. However, the preference of Mn for tetrahedral sites in manganese titanium oxides, coupled with the unusual degree of distortion of the *A* site for slag III (as noted above this is the largest and most distorted of the *A* sites for the materials studied herein), is a strong argument for placing Mn at the *A* site. Examples of reduced titanium manganese oxides with manganese in either extremely asymmetric octahedral or tetrahedral sites are Mn_2TiO_4 and $MnTi_2O_5$ (*19*). Assuming this to be true, site *B* is then 100% Ti occupied and all iron must be located on the *A* site. This is confirmed by the Mossbauer effect data which indicates that all the iron in the pseudobrookite structure for slag III is located on a single site. This relegates all the iron, and a mixture of Mn and Ti, to the *A* site. If we fix the amount of Mn, Ti, and Fe located at the *A* site (from the elemental composition), the calculated scattering length for this site is 0.12×10^{-12} cm. This is within 3 standard deviations of the observed neutron scattering length. This material is unique with regard to the other three samples in that it (a) contains manganese and (b) is apparently cation deficient, since the occupancies of the *A* site do not add to 1.0.

In a similar manner, the cation distributions of sample slag IV can also be calculated. The Mossbauer effect data indicate that there is only one type of ferrous ion in the pseudobrookite structure. Since all the iron is located at a single site (site *A*), Mg must be distributed between both metal sites. Since there are two metals at site *B* (Mg and Ti) one can calculate the site population assuming 100% total (Mg + Ti) occupation. Placing the balance of Mg, Fe, and Ti at site *A*, the calculated scattering length for site *A* is 0.28×10^{-12} cm. Again, this is within 3 standard deviations of the observed neutron scattering length (0.26×10^{-12} cm).

The Mg ion distributions for II and IV differ significantly from that of iron. This is noteworthy because earlier crystallographic site refinements of iron magnesium titanium oxides of the pseudobrookite structure based on X-ray diffraction data have always assumed that iron and magnesium occupancies for any given site are equal (*5, 6*). The results presented here demonstrate that this is an erroneous assumption.

An earlier study by Grey and Ward (*1*) of the solid–solution of $FeTi_2O_5/Ti_3O_5$, in which X-ray diffraction and Mossbauer effect spectroscopy were utilized to characterize a range of compounds ($Fe_{1-x}Ti_{2+x}O_5$, $0 < x < 1$), can be compared with the results of sample I (Table VI). For the series $x = 0.55$ to $x = 0$, the trends in the lattice parameters a, b, and c are 3.785 to 3.757, 9.798 to 9.790, and 10.013 to 10.079, respectively. It is clear that I ("Fe Ti_2O_5," $a = 3.7498$, $b = 9.8057$, $c = 10.0675$ Å) does not fall in the range of elemental composition studied by Grey and Ward. This is further supported by the presence of very small amounts of TiO_2 found in the mixtures examined herein, suggesting that the compounds I and II are iron rich with respect to the "as prepared" stoichiometries. These differences make the direct comparison of Mossbauer effect data (three quadrupole split doublets for I and II) from the two experiments problematical.

Interestingly enough, the cell parameters of "$Fe_{0.45}Ti_{2.55}O_5$" of Grey and Ward (*1*) closely match those of slag III ($Mn_{.05}Fe_{.33}Ti_{2.52}O_5$). For $Fe_{0.45}Ti_{2.55}O_5$, 75% of the iron ($Fe_{0.34}$) was identified as located on the "*A*" site; this agrees exactly with the total ferrous ion population found on site *A* for slag III, the only difference between the materials being the Mn occupation of site *B* (in place of iron).

Summary

Four iron titanium oxide compounds ($M_{1-x}Ti_{2+x}O_5$, $-0.1 < x < 0.52$, M = Fe, Mg, Mn) possessing the pseudobrookite (AB_2O_5) structure have been synthesized under two different sets of conditions at two temperatures (1200 and >1700°C). For the materials prepared at the lower temperature the *B* site is predominantly, but not 100%, occupied by Ti, while the *A* sites contain Fe, Ti, Mg, Mn, or a mixture thereof. Thus a "disordered" model best describes these low temperature structures. Additionally, it has been found that Mg and Fe occupancies of the *A* and *B* site are not identical.

At elevated synthesis temperatures (>1700°C) under reducing conditions, Mossbauer effect data indicate that no iron is found at the "*B*" site. Only at these higher temperatures can an "ordered" model be considered an accurate description of the cation distributions in these compounds. These results suggest that the thermodynamics that determine cation distributions in these materials is temperature dependent in the 1200–1700°C range, and that an accurate determination of the correct cation distributions (via neutron diffraction and/or MES) would determine the thermal history of naturally occurring ferrous titanium oxides.

Acknowledgments

The authors thank BP America and QIT Fer et Titane for permission to publish this work. The Intense Pulsed Neutron Source at Argonne National Laboratory is a user facility operated by the Department of Energy, contract No. W-31-109-ENG-38.

References

1. I. E. Grey and J. Ward, *J. Solid State Chem.* **7,** 300 (1973).
2. L. Pauling, *Z. Kristallogr.* **73,** 97 (1930), other models have also been proposed for pseudobrookite, by S. Muranka, T. Shirjo, Y. Bando and T. Takoda, *J. Phys. Soc., Japan* **30,** 890 (1971) and M. Hammelin, *Bull. Chem. Soc., France* **5,** 1559 (1958).
3. (a) J. B. MacChesney and A. Muan, *Amer. Mineral.* **46,** 572 (1961). (b) A. E. Grau, *Canad. Metall. Q.* **18,** 313 (1979).
4. G. S. Zhdanov and A. V. Rusakov, *Tr. Inst. Kristollogr. Akad. Nauk. USSR* **9,** 165 (1974).
5. J. R. Smyth, *Earth Planet. Sci. Lett.* **24,** 262 (1974).
6. B. A. Wechsler, *Amer. Mineral.* **62,** 913 (1977).
7. B. A. Wechsler, C. T. Prewitt, and J. J. Pike, *Earth Planet. Sci. Lett,* **29,** 91 (1976).
8. M. D. Lind and R. M. Housley, *Science* **175,** 521 (1972).
9. J. F. W. Bowles, *Amer. Mineral.* **73,** 1377 (1988).
10. R. A. Young, "National Bureau of Standards Special Publication 567 (1979) and references therein.
11. (a) J. R. Hauman, R. T. Daley, T. G. Worlton,

AND R. K. CRAWFORD, *IEEE Trans. Nucl. Sci.* **NS-29,** 62 (1982). (b) R. B. VON DREELE, J. D. JORGENSEN, AND C. G. WINDSOR, *J. Appl. Crystallogr.* **15,** 581 (1982). (c) J. D. JORGENSEN AND J. FABER, "ICANS-II, Proc. VIth Int. Collab. Adv. Neutron Sources, Argonne Natl. Lab., June 28–July 2, 1982," ANL-82-80 (1983). The equation relating time-of-flight (TOF) to d-value is TOF = d^* DIFC + d^{2*}DIFA + ZERO; for the GPPD, DIFC = 10453., DIFA = −2.59, ZERO = −13.50, and for the SEPD, DIFC = 7571.2, DIFA = −1.51, ZERO = −9.57.

12. G. J. LONG, T. E. CRANSHAW, AND G. LONGWORTH, *Mossbauer-Effect Reference Data Journal* **6,** 42 (1983).
13. F. I. TOROMANOFF AND F. HABASHI, *J. Less-Common Met.* **97,** 317 (1984).
14. A. F. WELLS, "Structural Inorganic Chemistry," 5th ed., p. 564, Oxford Univ. Press, London/New York (1983).
15. A. NAVROTSKY, *Amer. Mineral.* **60,** 249 (1975).
16. D. S. GOLDMAN AND D. E. BEWLEY, *J. Amer. Ceram. Soc.* **68,** 691 (1985).
17. (a) S. K. BANERJEE, W. O'REILLY, T. C. GIBB, AND N. N. GREENWOOD, *J. Phys. Chem. Solids* **28,** 1423 (1967). (b) M. J. ROSSITER AND P. T. CLARKE, *Nature (London)* **207,** 402 (1965). (c) R. VANLEERBERGHE AND R. E. VANDENBERGHE, *Hyperfine. Interact.* **23,** 75 (1985).
18. Based on MES and diffraction data the ferrous ion distribution for II is $(Fe_{.48}Ti_{.5})(Mg_{.6}Fe_{.08}Ti_{1.3})O_5$ (A/B = 6), this has been rounded off to $(Fe_{.5}Ti_{.5})(Mg_{.6}Fe_{.1}Ti_{1.3})O_5$ (A/B = 5).
19. (a) E. F. BERTAUT AND H. VINCENT, *J. Solid State Chem.* **6,** 269 (1968). (b) A. LECERF AND A. HARDY, *Compt. Rend. Hebd. Seances Acad. Sci.* **252,** 131 (1961).